Chinese Chemical Letters 33 (2022) 374–377

Contents lists available at ScienceDirect

Chinese Chemical Letters

journal homepage: www.elsevier.com/locate/cclet

# Ir nanoclusters confined within hollow MIL-101(Fe) for selective hydrogenation of $\alpha,\beta$-unsaturated aldehyde

Qinglin Liu[a,1], Qian Liu[a,1], Yurong Chen[a], Yinle Li[a], Hui Su[b], Qinghua Liu[b], Guangqin Li[a,*]

[a] MOE Laboratory of Bioinorganic and Synthetic Chemistry, Lehn Institute of Functional Materials, School of Chemistry, Sun Yat-sen University, Guangzhou 510275, China
[b] National Synchrotron Radiation Laboratory, University of Science and Technology of China, Hefei 230026, China

ARTICLE INFO

*Article history:*
Received 31 March 2021
Revised 8 May 2021
Accepted 17 June 2021
Available online 24 June 2021

*Keywords:*
Iridium
Hollow metal–organic frameworks
Selective hydrogenation
$\alpha,\beta$-Unaturated aldehyde
Heterogeneous catalysis

ABSTRACT

Although the selective hydrogenation of $\alpha,\beta$-unsaturated aldehyde to unsaturated alcohol (UOL) is an extremely important transformation, it is still a great challenge to achieve high selectivity to UOL due to thermodynamic favoring of the C=C hydrogenation over the C=O hydrogenation. Herein, we report that iridium nanoclusters (Ir NCs) confined within hollow MIL-101(Fe) expresses satisfied reaction activity (93.9%) and high selectivity (96.2%) for the hydrogenation of cinnamaldehyde (CAL) to cinnamyl alcohol (COL) under 1 bar $H_2$ atmosphere and room temperature. The unique hollow structure of MIL-101(Fe) benefits for the fast transport of reactant, ensuring the comparable reaction activity and better recyclability of Ir@MIL-101(Fe) than the counterparts which Ir NCs were on the surface of MIL-101(Fe). Furthermore, The X-ray photoelectron spectroscopy data indicates the electropositive Ir NCs, owing to the electron transfer from Ir to MIL-101(Fe), can interact with oxygen lone pairs, and Fourier transform infrared spectrum shows the Lewis acid sites in MIL-101(Fe) can strongly interact with C=O bond, which contributes to a high selectivity for COL. This work suggests the considerable potential of synergetic effect between hollow MOFs and metal nanoclusters for selective hydrogenation reactions.



The selective hydrogenation of $\alpha,\beta$-unsaturated aldehyde (UAL) to unsaturated alcohol (UOL) is a significant process in petrochemicals, pharmaceuticals and fragrances [1-4]. Nevertheless, since the production of saturated aldehydes is more favorable over unsaturated alcohols from the view of thermodynamics [5,6], it is extremely difficult to achieve high selectivity to UOL. Significant efforts have been devoted towards the development of highly UOL-selective catalysts [7-13], among which a great amount of noble metal based catalysts for selective hydrogenation of UAL have been made great progress. Among the noble metals, iridium (Ir) possesses the highest intrinsic selectivity to UOL [14]. However, pure Ir nanoparticles still showed unsatisfied selectivity in selective hydrogenation of UAL. In addition, the surface energy of metal nanoclusters (NCs) is very high, pure metal NCs are easy to aggregate in the reaction process, leading to a loss of activity [15-18].

Recently, metal-organic frameworks (MOFs) supported metal nanoparticles have attracted tremendous research interest because the micropores of MOFs can not only prevent the nanoparticles from aggregation and growth but also serve as a transfer path for the reaction substrates/products [19-26]. Moreover, compared with other porous materials such as zeolites and porous carbons, MOFs contain a large number of metal centers, which may interact with reactants to improve selectivity or catalyze the reaction directly [27-35]. Tang's group synthesized MIL-101(Fe)@Pt and achieved 86.4% selectivity to UOL, further suggested that MIL-101(Fe) can serve as effective selectivity regulator [28]. Hence, with MIL-101(Fe) as a protective layer and selectivity regulator, Ir NCs hybridized with MIL-101(Fe) were expected to exhibit an excellent activity and selectivity for hydrogenation of UAL to obtain high yield of UOL.

Herein, we have synthesized the hollow MIL-101(Fe) on preformed Ir NCs to generate Ir@MIL-101(Fe) composite. The obtained Ir@MIL-101(Fe) exhibits excellent performance in selective hydrogenation of a model molecule of $\alpha,\beta$-unsaturated aldehyde, cinnamaldehyde (CAL), with 93.9% conversion in 4 h and 96.2% selectivity towards cinnamyl alcohol (COL), as well as high durability after 5 successive cycles, all which are much better than those of Ir NCs and physical mixture Ir/MIL-101(Fe) catalysts. On one hand, the Lewis acid sites in MIL-101(Fe) are capable to interact with the aldehyde group in CAL and electropositive Ir NCs might preferential absorb the electronegative oxygen atom in C=O group, both of which can promote the selectivity for COL. On the other hand, the

* Corresponding author.
*E-mail address:* liguangqin@mail.sysu.edu.cn (G. Li).
[1] These authors contributed equally to this work.

https://doi.org/10.1016/j.cclet.2021.06.047
1001-8417/

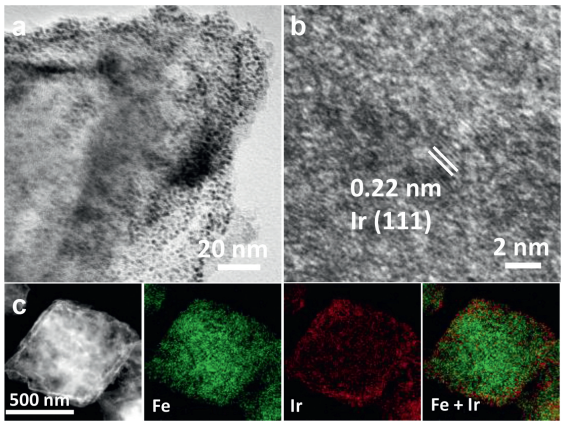


**Scheme 1.** Synthetic route to generating hollow Ir@MIL-101(Fe).

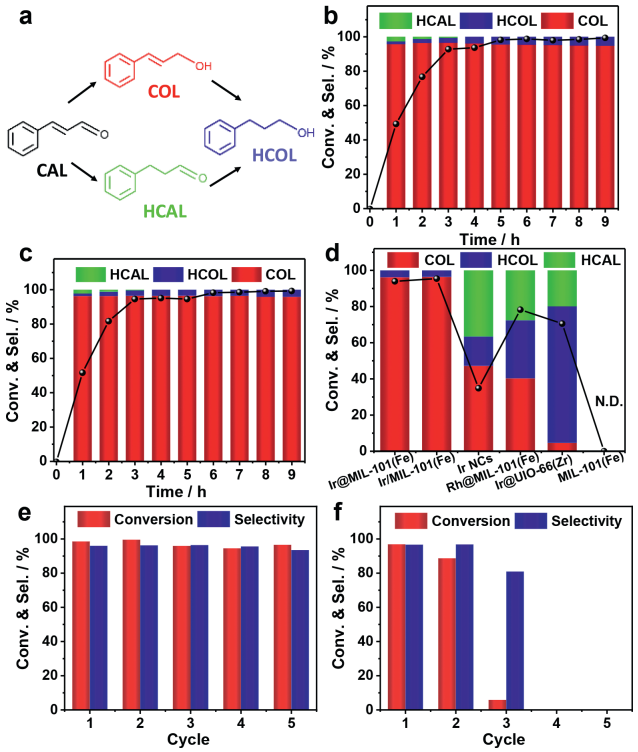


**Fig. 1.** (a, b) HRTEM images of Ir@MIL-101(Fe) samples. (c) HAADF-STEM image and the corresponding elemental mapping images of Ir@MIL-101(Fe).

special hollow structure of MIL-101(Fe) shortens the diffusion distance of reactants and remained the excellent hydrogenation.

As schematically illustrated in Scheme 1, the Ir@MIL-101(Fe) was synthesized by two processes. Firstly, the metal precursor salt was reduced using PVP as stabilizer and ethylene glycol as reductant and solvent to obtain Ir NCs, with the average size of 1.7 nm (Fig. S1 in Supporting information). Then the MIL-101(Fe) was grown *in situ* with the addition of Ir NCs in the precursor solution to obtain Ir NCs confined into hollow MIL-101(Fe) [29]. The structures and morphologies of as-prepared specimens were examined by powder X-ray diffraction (XRD), scanning electron microscopy (SEM) and high-resolution transmission electron microscopy (HRTEM). As shown in Fig. S2a (Supporting information), the XRD pattern of Ir@MIL-101(Fe) matched well with the MIL-101(Fe), no clear diffraction peaks of the Ir NCs were observed, due to the ultrafine size of the nanoclusters, which was consistent with HRTEM images (Fig. 1a) [30,36]. As for morphology, the surface of Ir@MIL-101(Fe) was a little bit rough compared with MIL-101(Fe) (Figs. S2b and S3 in Supporting information), owing to the existence of Ir NCs may slightly affecting the nucleation process of MOFs. The HRTEM images showed a lattice fringe of 0.22 nm corresponding to the (111) plane of the Ir metallic, and no observable aggregation on the external surface of MIL-101(Fe) (Figs. 1a and b). To test the element distribution of Ir@MIL-101(Fe), energy-dispersive X-ray spectroscopy (EDS) elemental mappings were carried out, and the Ir element was found to be mainly distributed on the near-surface of MIL-101(Fe) (Fig. 1c), which might shorten the diffusion distance of reactants on the surface of MIL-101(Fe) to the metal active site and thus facilitate the reaction rate. The actual Ir content in Ir@MIL-101(Fe) was quantitatively determined to be 5.3 wt% by inductively coupled plasma mass spectrometry (ICP-MS), listed in Table S1 (Supporting information). According to the $N_2$ adsorption isotherms (Fig. S4a in Supporting information), the Brunauer–Emmett–Teller (BET) surface area and total pore volume of Ir@MIL-101(Fe) decreased to 42.2 $m^2/g$ and 0.09 $cm^3/g$, compared to pure MIL-101(Fe) (664.1 $m^2/g$ and 0.38 $cm^3/g$), attributed to the formation of mesoporous in MIL-101(Fe). Furthermore, the pore-size distribution curve in Fig. S4b (Supporting information) also displayed the existence of mesoporous [30,37]. These results confirmed that most of the Ir NCs were indeed encapsulated inside the MOFs [38]. Moreover, Ir@MIL-101(Fe) with different hydrothermal times were synthesized. As shown in Fig. S5 (Supporting information), with the increase of hydrothermal time, the inner part of MIL-101(Fe) gradually became transparent, indicating hollow MOFs were formed. Since there is PVP on the surface of Ir NCs, PVP will dissolve in the growth solution during the hydrothermal reaction, and then act as metal-coordinating bulky polymer during the formation of MIL-101(Fe) domains to induce partial disruption of imidazole-Fe(III) catenation process and generate high mesoporosity in the resulting MIL-101(Fe) [39], which was consistent with pore-size distribution curve of Ir@MIL-101(Fe) (Fig. S4b in Supporting information).

To demonstrate the generality of our approach, Rh NCs confined within MIL-101(Fe) were also synthesized. The synthesis method of Rh@MIL-101(Fe) was similar to that of Ir@MIL-101(Fe), in which MIL-101(Fe) was *in situ* growth with the Rh NCs in the precursor solution to build hollow Rh@MIL-101(Fe) structures. The XRD patterns, SEM and HRTEM images, and $N_2$ adsorption isotherms of Rh@MIL-101(Fe) were shown in Figs. S6, S7 and S10 (Supporting information). Resembled to that of Ir@MIL-101(Fe), the BET surface areas of Rh@MIL-101(Fe) (Table S2 in Supporting information) was far less than those of the parent MIL-101(Fe), due to the formation of mesoporous MIL-101(Fe), which illustrated the generality of our new strategy for preparing the hollow metal@MIL-101(Fe) catalysts. In order to explore the role of MOFs, Ir@UIO-66(Zr) was synthesized for comparison [40]. The detailed information of Ir@UIO-66(Zr) was shown in Figs. S8-S10 (Supporting information).

Selective hydrogenation of $\alpha,\beta$-unsaturated aldehyde is very important in chemical industry. The hydrogenation of an $\alpha,\beta$-unsaturated aldehyde, CAL, is selected to explore the possible catalytic performance of Ir@MIL-101(Fe). As illustrated in Fig. 2a, CAL is hydrogenated to COL or hydrocinnamaldehyde (HCAL), and subsequently further hydrogenated to hydrocinnamyl alcohol (HCOL). Here, the hydrogenation of CAL was carried out under 1 bar $H_2$ pressure at room temperature. The conversion of CAL and selectivity for COL as a function of reaction time over Ir@MIL-101(Fe) were shown in Fig. 2b. After 4 h reaction, the conversion of CAL achieved 93.9%, with high selectivity of desired product COL (96.2%). When the reaction time was prolonged, the overhydrogenated product HCOL could not be observed, confirming the extraordinary product selectivity. As shown in Table S3 (Supporting information), the selectivity of Ir@MIL-101(Fe) is better than that of the Ir-based catalyst reported previously, which is comparable to the most ad-

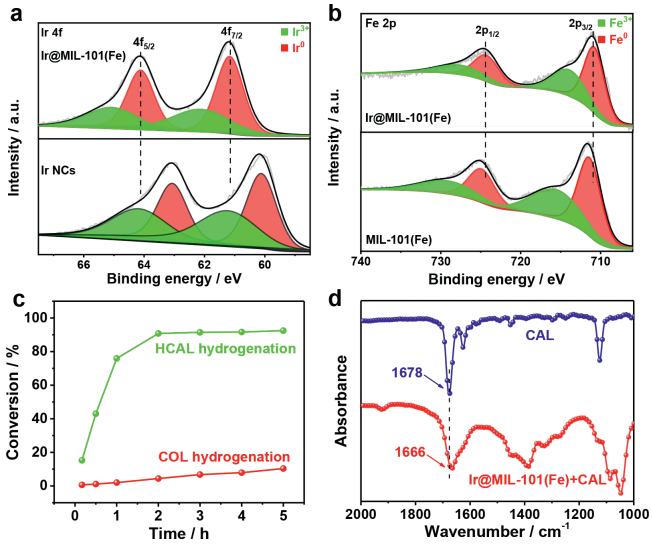


**Fig. 2.** (a) Schematic CAL hydrogenation. CAL hydrogenation performances of (b) Ir@MIL-101(Fe) and (c) Ir/MIL-101(Fe). (d) Product selectivity (Sel.) and conversion (Conv.) at 4 h for the CAL hydrogenation over different catalysts. (e) Recyclability of Ir@MIL-101(Fe) and (f) Ir/MIL-101(Fe) for hydrogenation of CAL. Reaction condition: Cinnamyl aldehyde (0.1 mmol), catalyst (15 mg), isopropanol (2.5 mL), water (2.5 mL), 30 °C, 1 bar $H_2$ atmosphere, 4 h.

vanced catalyst reported recently. To investigate whether the Ir active site was decreased after covering MOFs, Ir/MIL-101(Fe) was prepared by just mechanically mixing the pre-synthesized Ir NCs and MIL-101(Fe) (Fig. S11 in Supporting information). As observed in Fig. 2c, the similar catalytic activity of Ir/MIL-101(Fe) compared to Ir@MIL-101(Fe) inferred that the Ir NCs inside hollow MIL-101(Fe) maintained instinct catalytic ability, which attributed to the fasten transport speed and the shorten diffusion distance of reactants to the metal active site [36,41]. Moreover, Ir@MIL-101(Fe) and Ir/MIL-101(Fe) gave the higher selectivity for COL over pure Ir NCs (47.2%), Rh@MIL-101(Fe) (40.3%) and Ir@UIO-66(Zr) (4.6%) (Fig. 2d). Besides, less than 1% conversion of CAL was detected when catalyzed by MIL-101(Fe), which could be considered as a negligible influence on the hydrogenation reaction. The detailed catalysis results were listed in Table S4 (Supporting information). Above results indicated that synergistic effect of Ir NCs and the MIL-101(Fe) support may be the key factor for high yield of COL.

For the recyclability was another critical factor to evaluate the catalytic performance of catalysts, the stability tests of Ir@MIL-101(Fe) and Ir/MIL-101(Fe) for selective hydrogenation of CAL were carried out. As seen in Fig. 2e, no appreciable loss in activity and selectivity was observed in Ir@MIL-101(Fe) in up to five runs. On the contrary, when it came to the third cycle, the activity of Ir/MIL-101(Fe) declined sharply and the selectivity dropped to 81.0% (Fig. 2f). This is because the Ir active sites in Ir/MIL-101(Fe) probably leached and aggregated during the reaction [42], while the Ir NCs confined within MIL-101(Fe) were immune to this problem, leading to great recyclability. It is worth mentioning that confining Ir NCs within MIL-101(Fe) cavities did not sacrifice their activity, since the turnover frequency (TOF) values of Ir@MIL-101(Fe) and Ir/MIL-101(Fe) were similar (Fig. S12 in Supporting information). The mesopores in MIL-101(Fe) provided enough space for the transport and diffusion of substrates and products, thus ensuring the efficient reaction [39]. Another factor attributed to high activity was that Ir NCs were mainly loaded in the near surface of MIL-101(Fe), which afforded a short diffusion distance of the reactants from the MIL-101(Fe) surface to the highly exposed NCs active sites [43]. In addition, though some active sites of Ir NCs were covered when loaded in or on the MIL-101(Fe), the TOF of Ir@MIL-101(Fe)

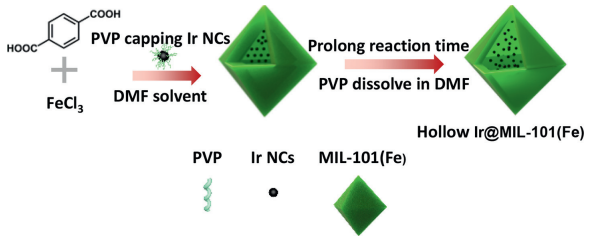


**Fig. 3.** XPS profiles of Ir and Fe in different catalysts. (a) Ir 4f level. (b) Fe 2p level. The catalysts investigated were pure Ir NCs, MIL-101(Fe) and Ir@MIL-101(Fe). (c) HCAL and COL hydrogenation performances of Ir@MIL-101(Fe). (d) FT-IR spectra for CAL adsorption on Ir@MIL-101(Fe).

and Ir/MIL-101(Fe) outperformed pure Ir NCs (Fig. S12), which may be attributed to hydrogen spillover effect on the surface of MIL-101(Fe) [44]. To investigate the universality of Ir@MIL-101(Fe), hydrogenation of different $\alpha,\beta$-unsaturated aldehydes were tested. As shown in Table 1, almost all the substrates can reach over 90% selectivity to corresponding UOL. Above results fully suggest that Ir@MIL-101(Fe) is an excellent catalyst for selective hydrogenation of $\alpha,\beta$-unsaturated aldehydes.

Since surface chemical structure of catalysts have a considerable influence on the catalytic behavior [45,46], the electronic properties of Ir and Fe were characterized by X-ray photoelectron spectroscopy (XPS). Ir 4f spectrum of Ir@MIL-101(Fe) and Ir NCs clearly demonstrated that most of Iridium remained $Ir^0$ valance but a portion of $Ir^{3+}$ material existed on the surface, due to the oxidation in the air (Fig. 3a) [47]. The Fourier transforms of extended X-ray absorption fine structure (FT-EXAFS) further verified the existence of Ir metallic and oxide, since the peak of Ir-Ir bond and Ir-O bond were clearly found in the Ir $L_3$-edge (Fig. S13 in Supporting information). Compared with the binding energy of $Ir^0$ in Ir NCs (63.1 eV, $4f_{5/2}$), the higher binding energy in Ir@MIL-101(Fe) (64.1 eV, $4f_{5/2}$) indicated the lower electron density of Ir after confining within the hollow MIL-101(Fe). As for the binding energy of $Fe^{3+}$ in Ir@MIL-101(Fe), the peak of Fe $2p_{3/2}$ obviously shifted from 716.0 eV to 714.5 eV after immobilization of Ir NCs, confirmed the electron transfer from Ir to MIL-101(Fe) (Fig. 3b). Since the O atom in C=O was electronegative, electropositive Ir NCs in Ir@MIL-101(Fe) may be able to absorb the C=O bond to activate it [48,49], resulting in high selectivity towards COL.

In order to deeply investigate the reason for excellent COL selectivity, hydrogenation using COL and HCAL as the substrate were performed over Ir@MIL-101(Fe). As expected, the hydrogenation rate of C=O bond was clearly faster than that of C=C bond (Fig. 3c), attributing to enhance the selectivity of COL and avoid the over hydrogenation to a great extent. To find out the mechanism for selective hydrogenation of CAL, the Fourier transform infrared (FT-IR) spectroscopy was used to examine the adsorption of CAL on Ir@MIL-101(Fe). As shown in Fig. 3d, FT-IR survey showed an obvious redshift of the $\upsilon_{C=O}$ bond of CAL after mixing with Ir@MIL-101(Fe), confirming strong interaction between the C=O bond of CAL and Ir@MIL-101(Fe) [28,50]. Similar adsorption behaviors were also observed when mixing CAL with Ir/MIL-101(Fe) and MIL-101(Fe) (Fig. S14 in Supporting information). These revealed that the synergistic effect of electropositive Ir NCs and the aldehyde activator MIL-101(Fe) was key to preferentially hydrogenate aldehyde group and maintaining high selectivity towards COL.

In summary, we have successfully developed a new method for confining metal NCs within hollow MOFs *via in-situ* growth of MOFs with metal NCs in the precursor solution. Interestingly, as-prepared Ir@MIL-101(Fe) exhibited impressive activity (93.9%), selectivity (96.2%) as well as great recyclability for the hydrogenation of CAL to COL under mild conditions. The electropositive Ir NCs,

**Table 1**
Hydrogenation of $\alpha,\beta$-unsaturated aldehyde catalyzed by Ir@MIL-101(Fe).

| Entry | Substrate | Time (h) | Conv. (%) | Sel. of UOL (%) | Yield of UOL (%) |
|---|---|---|---|---|---|
| 1 | 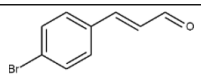 | 4 | 90.2 | 98.0 | 88.4 |
| 2 | 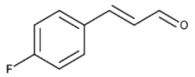 | 5 | 94.1 | 88.7 | 83.5 |
| 3 | 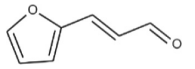 | 8 | >99.9 | >99.9 | >99.9 |
| 4 | 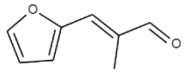 | 8 | 92.7 | 99.0 | 91.8 |
| 5 | 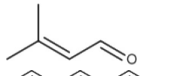 | 8 | 83.1 | >99.9 | 83.1 |
| 6 | 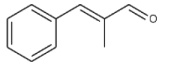 | 8 | 83.2 | 97.8 | 81.4 |
| 7 | 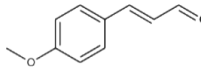 | 8 | 97.9 | 90.8 | 88.9 |

Reaction condition: Substrate (0.1 mmol), catalyst (15 mg), isopropanol (2.5 mL), water (2.5 mL), 30 °C, 1 bar $H_2$ atmosphere.

owing to the electron transfer from Ir to MIL-101(Fe), prefer to interact with oxygen lone pairs of aldehyde group and the Lewis acid sites in MIL-101(Fe) can strongly interact with C=O bond, both factors are attributed to high selectivity to COL. This work provides an efficient strategy to prepare promising materials for enhanced selective hydrogenation of $\alpha,\beta$-unsaturated aldehyde.

## Declaration of competing interests

The authors declare that they have no known competing financial interests or personal relationships that could have appeared to influence the work reported in this paper.

## Acknowledgments

This work was supported by National Key R&D Program of China (No. 2018YFA0108300), the Overseas High-level Talents Plan of China and Guangdong Province, the 100 Talents Plan Foundation of Sun Yat-sen University, the Program for Guangdong Introducing Innovative and Entrepreneurial Teams (No. 2017ZT07C069), the Fundamental Research Funds for the Central Universities, and the NSFC Projects (Nos. 21905315 and 22075321).

## Supplementary materials

Supplementary material associated with this article can be found, in the online version, at doi:10.1016/j.cclet.2021.06.047.

## References

[1] H. Wang, S. Bai, Y. Pi, et al., ACS Catal. 9 (2018) 154–159.
[2] N. Zhang, Q. Shao, P. Wang, et al., Small 14 (2018) 1704318.
[3] C.A. Schoenbaum, D.K. Schwartz, J.W. Medlin, Acc. Chem. Res. 47 (2014) 1438–1445.
[4] J. Zhang, Z. Gao, S. Wang, et al., Nat. Commun. 10 (2019) 4166.
[5] Y. Bonita, V. Jain, F.Y. Geng, et al., Appl. Catal. B 277 (2020) 119272.
[6] Y. Lou, Y. Zheng, X. Li, et al., J. Am. Chem. Soc. 141 (2019) 19289–19295.
[7] S. Tsang, N. Cailuo, ACS Nano 2 (2008) 2547–2553.
[8] A.B. Merlo, B.F. Machado, V. Vetere, et al., Appl. Catal. A: Gen. 383 (2010) 43–49.
[9] Q. Yang, Y. Zhu, Appl. Catal. A: Gen. 369 (2009) 67–76.
[10] B. Wu, H. Huang, J. Yang, et al., Angew. Chem. Int. Ed. 51 (2012) 3440–3443.
[11] I. Cano, A.M. Chapman, A. Urakawa, et al., J. Am. Chem. Soc. 136 (2014) 2520–2528.
[12] P. Aich, H. Wei, B. Basan, et al., J. Phys. Chem. C 119 (2015) 18140–18148.
[13] Y. Cao, J. Guerrero-Sańchez, I. Lee, et al., ACS Catal. 10 (2020) 3431–3443.
[14] A. Giroir-Fendler, D. Richard, P. Gallezot, Stud. Surf. Sci. Catal. 41 (1988) 171–178.
[15] D. Chen, W. Yang, L. Jiao, et al., Adv. Mater. 32 (2020) 2000041.
[16] Y. Chen, B. Gu, Nat. Commun. 10 (2019) 3462–3471.
[17] S. Gao, H. Zhao, J. Feng, et al., Ind. Eng. Chem. Res. 56 (2017) 10631–10638.
[18] M. Mao, M. Zhang, D. Meng, et al., ChemCatChem 12 (2020) 3530–3536.
[19] Y. Ma, Y. Lu, G. Hai, et al., Sci. Bull. 65 (2020) 658–669.
[20] J. Long, H. Liu, S. Wu, et al., ACS Catal. 3 (2013) 647–654.
[21] X. Xie, L. Peng, H. Yang, et al., Adv. Mater. (2021) 2101038.
[22] L. Ning, M. Zhang, S. Liao, et al., Adv. Funct. Mater. 27 (2017) 1606215.
[23] Y. Sun, Z. Xue, Q. Liu, et al., Nat. Commun. 12 (2021) 1369.
[24] J. Yang, F. Zhang, H. Lu, Nat. Commu. 54 (2015) 10889–10893.
[25] H. Yang, X. Wang, Adv. Mater. 31 (2018) 1800743.
[26] T. He, B. Ni, S. Zhang, Small 14 (2018) 1703929.
[27] Q. Liu, Y. Li, J. Mater. Chem. A 8 (2020) 11442–11447.
[28] M. Zhao, K. Yuan, Y. Wang, et al., Nature 539 (2016) 76–80.
[29] V. Bakuru, S. Kalidindi, Chem. Eur. J. 23 (2017) 16456–16459.
[30] Z. Guo, C. Xiao, ACS Catal. 4 (2014) 1340–1348.
[31] S. Ji, Y. Chen, S. Zhao, et al., Angew. Chem. Int. Ed. 58 (2019) 4271–4275.
[32] H. Ye, H. Zhao, Y. Jiang, et al., ACS Appl. Nano Mater. 3 (2020) 12260–12268.
[33] Y. Chen, Y. Zhou, ACS Catal. 5 (2015) 2062–2069.
[34] X. Li, B. Zhang, L. Tang, et al., Angew. Chem. Int. Ed. 129 (2017) 16589–16593.
[35] B. Li, H.C. Zeng, Chem. Mater. 31 (2019) 5320–5330.
[36] H. Liu, L. Chang, ChemCatChem 8 (2016) 946–951.
[37] K. Yuan, T. Song, D. Wang, et al., Angew. Chem. Int. Ed. 57 (2018) 5708–5713.
[38] L. Li, W. Yang, Q. Yang, et al., ACS Catal. 10 (2020) 7753–7762.
[39] S. Dutta, N. Kumari, S. Dubbu, et al., Angew. Chem. Int. Ed. 132 (2020) 3444–3450.
[40] Y. Zhao, H. Zhou, W. Chen, et al., J. Am. Chem. Soc. 141 (2019) 10590–10594.
[41] Q. Yang, W. Liu, B. Wang, et al., Nat. Commun. 8 (2017) 14429.
[42] C. Stephenson, C. Whitford, P. Stair, et al., ChemCatChem 8 (2016) 855–860.
[43] A. Zhou, Y. Dou, ChemSusChem 13 (2019) 205–211.
[44] G. Li, H. Kobayashi, J.M. Taylor, et al., Nat. Mater. 13 (2014) 802–806.
[45] L. Lin, S. Yao, R. Gao, et al., Nat. Nanotechnol. 14 (2019) 354–361.
[46] J. Jiao, R. Lin, S. Liu, et al., Nat. Chem. 11 (2019) 222–228.
[47] S. He, L. Xie, M. Che, et al., J. Mol. Catal. A: Chem. 425 (2016) 248–254.
[48] S. Bai, L. Bu, J. Am. Chem. Soc. 140 (2018) 8384–8387.
[49] W. Cheong, W. Yang, J. Zhang, et al., ACS Appl. Mater. Interfaces 11 (2019) 33819–33824.
[50] S. Tian, M. Hu, Q. Xu, et al., Sci. China Mater. 64 (2020) 642–650.